

Quasi-two-dimensional hole ordering and dimerized state in the CuO₂-chain layers in Sr₁₄Cu₂₄O₄₁

M. Matsuda

The Institute of Physical and Chemical Research (RIKEN), Wako, Saitama 351-0198, Japan

T. Yoshihama and K. Kakurai

Neutron Scattering Laboratory, ISSP, University of Tokyo, Tokai, Ibaraki 319-1106, Japan

G. Shirane

Physics Department, Brookhaven National Laboratory, Upton, New York 11973

(Received 3 August 1998)

Neutron scattering experiments have been performed on Sr₁₄Cu₂₄O₄₁ which consists of both chains and ladders of copper ions. We observed that the magnetic excitations from the CuO₂ chain have two branches and that both branches are weakly dispersive along the *a* and *c* axes. The ω -*Q* dispersion relation as well as the intensities can be reasonably described by a random phase approximation with intradimer coupling between next-nearest-neighbor copper spins $J=11$ meV, interdimer coupling along the *c* axis $J_c=0.75$ meV, and interdimer coupling along the *a* axis $J_a=0.75$ meV. The dimer configuration indicates a quasi-two-dimensional hole ordering, resulting in an ordering of magnetic Cu²⁺ with spin- $\frac{1}{2}$ and nonmagnetic Cu, which forms the Zhang-Rice singlet. We have also studied the effect of Ca substitution for Sr on the dimer and the hole ordering.

75.25.+z, 75.10.Jm, 75.40.Gb

I. INTRODUCTION

Sr₁₄Cu₂₄O₄₁ consists of both two-leg ladders of copper ions and simple CuO₂ chains^{1,2} as shown in Fig. 1. Numerous experiments showed that the two-leg ladder has an excitation gap of ~ 35 meV,³⁻⁷ which is expected theoretically.⁸ An important feature of this compound is that stoichiometric Sr₁₄Cu₂₄O₄₁ contains hole carriers. It has been reported that most of the holes are localized in the chain and some exist in the ladder.⁹⁻¹¹ When Sr²⁺ sites are substituted by Ca²⁺ ions, total number of the holes in the sample is unchanged but holes in the chain are transferred from the chain to the ladder^{10,11} and the system shows an insulator-to-metal transition^{9,12}. Superconductivity was also observed in Sr_{0.4}Ca_{13.6}Cu₂₄O₄₁ below $T_c=10$ K under a high pressure of 3 GPa¹³.

In this paper we are only concerned with the magnetic properties in the chains. Figure 1(a) shows the CuO₂ chains in this compound. The copper ions are coupled by almost 90° Cu-O-Cu bond along the *c* axis. Each chain is well isolated from each other along the *a* and *b* axes. As mentioned above, there are localized holes in the chain. It is expected that the hole spins are localized at oxygen¹⁰ and couple with copper spins to form Zhang-Rice singlet¹⁴. The nonmagnetic Cu sites play an important role to form a dimerized state in the chain. First, the dimer is formed between next-nearest-neighbor Cu²⁺ spins along the *c* axis. The exchange interaction (~ 10 meV) is mediated via a nonmagnetic ZR singlet.^{5,15,16} Then the question is how the dimers are arranged and interact with each other. Matsuda *et al.*¹⁵ interpreted that each dimer is separated by one ZR singlet along the *c* axis (Model I) as shown in Fig. 1(c). They also interpreted that the excitations at low-*Q* ($L_{chain} < 0.4$) originate from a dimerized state in the chain and those at high-*Q* ($L_{chain} > 0.6$) from a dimerized state due to the interladder coupling since two branches were observed for the gap excitations at low-*Q* but only one branch at high-*Q*.

NMR studies revealed the microscopic properties of the dimerized state.^{5,17} It was reported that both magnetic Cu²⁺ and nonmagnetic ZR singlet exist in the chain. It was also found that a NMR peak originating from ZR singlet gradually splits into two peaks below ~ 200 K. The results were discussed with two dimer models. One is Model I mentioned above. This model was supported by Cox *et al.* by their x-ray measurements.¹⁸ In another model the dimers, which are formed between next-nearest-neighbor Cu²⁺ spins, are separated by two nonmagnetic ZR singlets along the *c* axis (Model II) as shown in Fig. 1(d). This model is consistent with the results of the electron diffraction study by Hiroi *et al.*¹⁹ in which the CuO₂ chains show a modulated structure with five times larger unit cell along the *c* axis in stoichiometric Sr₁₄Cu₂₄O₄₁. However, neither models cannot completely explain the NMR results.

Recently, two unpublished papers^{16,20} on neutron scattering experiments came to our attention. Eccleston *et al.*¹⁶ explained the modulation of the excitations and intensities along the *c* axis convincingly by a simple model of an alternating chain with weak interdimer coupling²¹ ($J_2/J_1 \sim -0.1$, where J_1 and J_2 are intradimer and interdimer

coupling, respectively), which is equivalent to Model II. It is noted that two parallel branches along the c axis are not separated in the experiments because of insufficient resolution. Regnault *et al.*²⁰ briefly reported the measurement of two parallel branches in a wide range of Q ($0.05 \leq L_{\text{chain}} \leq 0.925$) along the c axis, which suggested a weak coupling along the a direction. The specific coupling along the a direction was recently reported by Cox *et al.*¹⁸ in their synchrotron x-ray study of the charge ordering at low temperatures.

Since dimerized states sometimes occur in spin (S) $\frac{1}{2}$ one-dimensional Heisenberg antiferromagnets such as the spin-Peierls state, it is quite natural to assume that the dimerized state in the chain of $\text{Sr}_{14}\text{Cu}_{24}\text{O}_{41}$ is also caused by a quantum effect in $S=\frac{1}{2}$ one-dimensional Heisenberg antiferromagnet. On the other hand, almost isolated magnetic dimers were found in $\text{CaCuGe}_2\text{O}_6$ ^{22,23} even though the geometrical arrangement of the magnetic moments seems three-dimensional. It was also claimed that magnetic moments which are geometrically closest does not necessarily couple most dominantly in $\text{VODPO}_4 \cdot \frac{1}{2}\text{D}_2\text{O}$ ²⁴ and $(\text{VO})_2\text{P}_2\text{O}_7$ ²⁵ because of the strong superexchange pathways through a covalently bonded PO_4 group. These results suggest that unexpected pathways could become important in order to completely understand the magnetic properties of magnetic materials.

We have searched for a simple model of dimers with weak couplings along both c and a directions.²⁶ Somewhat surprisingly, a specific combination of the two couplings, as described by Leuenberger *et al.*²⁷ for $\text{Cs}_3\text{Cr}_2\text{Br}_9$, produces simple and elegant neutron scattering cross sections which describe properly the measured dispersion and intensities. In this paper, we have studied ω - Q dispersion relation perpendicular to the chain direction in considerable detail. By applying a random phase approximation (RPA) treatment, we found that the interdimer coupling along the a axis ($J_a=0.75$ meV) is also important²⁸ as well as the interdimer coupling along the c axis ($J_c=0.75$ meV). Model cross section will be given after the experimental data are presented. The dimer arrangement along the c axis is well described with Model II. The dimer configuration we found in this study indicates a quasi-two-dimensional hole ordering, resulting in an ordering of Cu^{2+} and ZR singlet in the ac plane. Ca substitution for Sr makes the magnetic excitation peaks broader as in the case of Y substitution²⁹ probably because the hole ordering is very sensitive to the hole number and the long-range dimer formation becomes disturbed.

II. EXPERIMENTAL DETAILS

The single crystals of $\text{Sr}_{14-x}\text{Ca}_x\text{Cu}_{24}\text{O}_{41}$ ($x=0$ and 3) were grown using a traveling solvent floating zone (TSFZ) method at 3 bars oxygen atmosphere. The dimension of the cylindrically shaped crystals is about $5 \times 5 \times 30$ mm³. The effective mosaic of the single crystal is less than 0.4° with the spectrometer condition as described below. The $\text{Sr}_{14}\text{Cu}_{24}\text{O}_{41}$ crystal is the same one as used in Ref. 15. It is expected that Sr and Ca are distributed homogeneously in $\text{Sr}_{11}\text{Ca}_3\text{Cu}_{24}\text{O}_{41}$ since the lattice constants systematically change and the linewidth of the nuclear Bragg peaks does not change when the ratio of Sr and Ca is changed. The lattice constants of $\text{Sr}_{14}\text{Cu}_{24}\text{O}_{41}$ and $\text{Sr}_{11}\text{Ca}_3\text{Cu}_{24}\text{O}_{41}$ are $a=11.472$ Å and $c=27.551$ Å and $a=11.430$ Å and $c=27.487$ Å at 15 K, respectively. The lattice constants are consistent with those obtained with powder samples.⁹

The neutron scattering experiments were carried out on the ISSP-PONTA spectrometer installed at the 5G beam hole of the Japan Research Reactor 3M (JRR-3M) at Japan Atomic Energy Research Institute (JAERI). The horizontal collimator sequences were $40'-40'-\text{S}-80'-80'$. The final neutron energy was fixed at $E_f=14.7$ meV. Pyrolytic graphite (002) was used as monochromator and analyzer. Contamination from higher-order beam was effectively eliminated using pyrolytic graphite filters after the sample. The single crystals were mounted in a closed cycle refrigerator and were oriented in the $(h,0,l)$ scattering plane. As described in Ref. 1, there are three different values for the lattice constant c ($c_{\text{universal}}=10 \times c_{\text{chain}}=7 \times c_{\text{ladder}}$). Since we will show the magnetic and structural properties in the chain, c_{chain} will be used to express Miller indices.

III. EXPERIMENTAL RESULTS

A. Magnetic excitations from $\text{Sr}_{14}\text{Cu}_{24}\text{O}_{41}$ chain

1. Low temperature dispersion

Figure 2 shows the typical neutron inelastic spectra at $(H,0,L)$ in $\text{Sr}_{14}\text{Cu}_{24}\text{O}_{41}$ measured at 15 K. One or two distinct excitation peaks are observed in the $(H,0,L)$ scattering plane as in the $(0,K,L)$ scattering plane which was previously reported in Ref^{15,29}. The solid lines at $(2,0,-0.20)$, $(2.75,0,-0.20)$, $(2,0,-0.75)$, and $(3,0,-0.75)$ are fits to two Gaussians and those at $(2,0,-0.70)$ and $(2.75,0,-0.70)$ are the fits to a single Gaussian. The excitation peak positions are changed when H or L is changed, meaning a dispersion along the a and c axes. The width of the

excitation peaks varies at different Q positions purely due to the resolution focussing effect. At $(3, 0, -0.75)$, where resolution focussing is almost perfect, the peak width has a resolution limited value of ~ 1 meV full width at half maximum. The observed excitation energies and energy-integrated intensities at $(2, 0, L)$ and $(3, 0, L)$ ($0.1 \leq L \leq 0.85$) are plotted in Figs. 3 and 4, respectively. The closed circles represent the data from the magnetic peaks with lower excitation energy and the open circles from the ones with higher excitation energy. The solid and broken lines are the results of model calculations, which will be presented in the next section. Both at $(2, 0, L)$ and $(3, 0, L)$ the dispersion relations are similar and has a periodicity of 0.2 r.l.u. along the c axis which is consistent with the results by Eccleston *et al.*¹⁶ and Regnault *et al.*²⁰ Actually the dispersion relation is almost identical to the one observed in the $(0, K, L)$ zone.¹⁵ The most interesting feature is that the intensities and the ratio of the two peaks are changed with H as well as L . The intensities of the excitation peaks with lower excitation energy are more intense than those with higher excitation energy at $(2, 0, L)$ ($L < 0.25$). On the other hand, the intensities of the excitation peaks with higher excitation energy are more intense than those with lower excitation energy at $(2, 0, L)$ ($L > 0.6$). The intensities at $(2, 0, L)$ are almost identical to those observed in the $(0, K, L)$ zone.¹⁵ The intensities at $(3, 0, L)$ show completely opposite behavior from those at $(2, 0, L)$. It is noted that the intensities in Ref. 16 is the sum of intensities from the two excitations.

Figures 5 and 6 show the observed excitation energies and energy-integrated intensities at $(H, 0, -0.2)$ and $(H, 0, -0.7)$ ($2 \leq H \leq 4$), respectively. The closed circles represent the data from the magnetic peaks with lower excitation energy and the open circles from the ones with higher excitation energy. The solid and broken lines are the results of model calculations, which will be presented in the next section. There also exists a dispersion along the a axis with a periodicity of 2 r.l.u. The two dispersion curves along the a axis do not run parallel as ones along the c axis but cross at $H = \frac{5}{2}$ and $\frac{7}{2}$. The intensities of the excitation peaks with lower excitation energy are larger than those with higher excitation energy in a range of $2 < H < 2.5$ and $3.5 < H < 4$ at $(H, 0, -0.2)$. On the other hand, in a range of $2.5 < H < 3.5$ the intensities of the excitation peaks with higher excitation energy are larger than those with lower excitation energy. The intensities at $(H, 0, -0.7)$ show completely opposite behavior from those at $(H, 0, -0.2)$. Thus, both the dispersion and the intensities depend on H and L , suggesting that there are nonnegligible magnetic correlations along the a axis in addition to those along the c axis.

2. Model Hamiltonian

In order to analyze the observed dispersion relation and energy-integrated intensities we used a model Hamiltonian for the dimers formed between next-nearest-neighbor Cu^{2+} spins which are weakly coupled along the a and c axes as shown in Fig. 7. The Hamiltonian involves three Heisenberg Hamiltonians with intradimer coupling J , interdimer coupling in the same chain J_c , and interdimer coupling between the adjacent chains J_a :

$$\hat{H} = J \sum_{\langle i, j \rangle} \mathbf{S}_i \cdot \mathbf{S}_j + J_c \sum_{\langle i, j \rangle'} \mathbf{S}_i \cdot \mathbf{S}_j + J_a \sum_{\langle i, j \rangle''} \mathbf{S}_i \cdot \mathbf{S}_j \quad (1)$$

Here, $\langle i, j \rangle$ and $\langle i, j \rangle'$ are nearest-neighbor and next-nearest-neighbor spins in the same chain, respectively. $\langle i, j \rangle''$ is nearest-neighbor spins between the adjacent chains. This type of dimers, namely weakly coupled dimers, can be well described with RPA. In fact, the magnetic excitations in $\text{Cs}_3\text{Cr}_2\text{Br}_9$ ²⁷ and $\text{BaCuSi}_2\text{O}_6$ ³⁰ are successfully described with RPA treatment. The dispersion relation is given by²⁷

$$\begin{aligned} \omega^{\text{acoustic/optic}}(\mathbf{q}) &= [J^2 + J \cdot R(T) (J_c \Gamma_c(\mathbf{q}) \pm J_a |\Gamma_a(\mathbf{q})|)]^{1/2}, \\ R(T) &= n_0 - n_1 = \frac{1 - \exp(-J/T)}{1 + 3\exp(-J/T)}, \\ \Gamma_c(\mathbf{q}) &= 2\cos(2\pi l), \\ \Gamma_a(\mathbf{q}) &= 2\cos(\pi h) \cdot \exp(i2\pi l\delta), \end{aligned} \quad (2)$$

where n_0 , n_1 , and δ are thermal populations of the singlet ground state and of the first excited triplet and the distance along the a axis between nearest-neighbor spins at the adjacent chains as shown in Fig. 7. The solid and broken lines in Figs. 3(a)-6(a) represent the calculated dispersion relation of the acoustic and optic modes, respectively. Equation (2) with $J=11$ meV, $J_a=0.75$ meV, and $J_c=0.75$ meV reproduces the observed data remarkably well. In this dispersion relation, the averaged excitation energy, the band width of each excitation mode, and the energy difference between the acoustic and optic modes are related with J , J_c , and J_a , respectively. J and J_c obtained in this experiment are consistent with those obtained by Eccleston *et al.*¹⁶ The sign of J_a is consistent with that in $\text{La}_{14-x}\text{Ca}_x\text{Cu}_{24}\text{O}_{41}$ which shows a long range magnetic ordering.^{31,32}

RPA treatment gives the dynamic structure factor²⁷ as the following.

$$\begin{aligned}
S(\mathbf{Q}, \omega) \propto & F^2(\mathbf{Q}) \cdot R(T) \cdot J \cdot [1 - \cos(\mathbf{Q} \cdot \mathbf{R})] \\
& \times \left[[1 + \cos(\boldsymbol{\rho} \cdot \boldsymbol{\tau} + \phi)] \frac{1}{\omega_{\text{acoustic}}(\mathbf{q})} \delta(\omega - \omega_{\text{acoustic}}(\mathbf{q})) \right. \\
& \left. + [1 - \cos(\boldsymbol{\rho} \cdot \boldsymbol{\tau} + \phi)] \frac{1}{\omega_{\text{optic}}(\mathbf{q})} \delta(\omega - \omega_{\text{optic}}(\mathbf{q})) \right]
\end{aligned} \tag{3}$$

where $\phi = 2\pi l\delta$, $\mathbf{Q} = \mathbf{q} + \boldsymbol{\tau}$ ($\boldsymbol{\tau}$ is a reciprocal wave vector), and \mathbf{R} is the vector connecting individual spins within a dimer. The factor $[1 - \cos(\mathbf{Q} \cdot \mathbf{R})]$ can be seen in the structure factor for isolated dimers. The acoustic and optic modes can be distinguished by the factor $[1 \pm \cos(\boldsymbol{\rho} \cdot \boldsymbol{\tau} + \phi)]$. The solid and broken lines in Figs. 3(b)-6(b) represent the energy-integrated intensities of the acoustic and optic modes calculated using Eq. (3), respectively. J , J_a , and J_c are fixed at the values mentioned above. δ is fixed at 0.77 which was determined by x-ray measurements at 50 K.¹⁸ Only adjustable parameter is the scale factor. The same scale factor was used for the intensities at $(2,0,L)$, $(3,0,L)$, $(H,0,-0.2)$, and $(H,0,-0.7)$. The energy-integrated intensities are described with the RPA theory reasonably well.

3. Temperature dependence

Figure 8 shows constant- Q scans at $(2,0,-0.1)$ and $(2,0,-0.6)$ as a function of temperature. The solid lines are the fits to two Gaussians. In the fitting the higher excitation energy at $(2,0,-0.1)$ and the lower excitation energy at $(2,0,-0.6)$ are fixed, which is confirmed with more intense excitation peaks at $(3,0,-0.1)$ and $(3,0,-0.6)$. It was assumed that the peak width and the intensity ratio of the two excitations are temperature independent. Temperature dependence of excitation energies and energy-integrated intensities are plotted in Fig. 9. The lower excitation energy at $(2,0,-0.1)$ becomes higher and the higher excitation energy at $(2,0,-0.6)$ becomes lower with increasing temperature. Furthermore, the intensities decrease with increasing temperature. Since there is a thermal factor $R(T)$ in Eqs. (2) and (3), the RPA calculation predicts the temperature dependence of the dispersion relation and the energy-integrated intensities. The dispersion becomes flatter with increasing temperature as shown in the inset of Fig. 9. because the interdimer couplings become negligible due to large thermal fluctuations and the dimers behave like isolated dimers. The intensity is proportional to $R(T)$ which decreases with increasing temperature. The solid lines in Fig. 9 are the results of calculations using Eq. (2) and (3). All the parameters J , J_a , J_c , δ , and scale factor are fixed at the values as determined above. The temperature dependences are fitted with the RPA calculation reasonably well although the observed intensity decreases more quickly than the calculated intensity does. This indicates that other factors in addition to thermal fluctuations disturb the dimers and the ordering of Cu^{2+} and ZR singlet. A gradual destruction of the ordering with increasing temperature suggested by NMR⁵ and x-ray measurements¹⁸ might cause the behavior.

4. Discussion

Now we discuss the relation between magnetic dimerization and structural distortion. As mentioned in Sec. I, Cox *et al.*¹⁸ performed synchrotron x-ray measurements on $\text{Sr}_{14}\text{Cu}_{24}\text{O}_{41}$ and observed superlattice Bragg peaks at $(0,0,l/4)$ and $(0,0,l/2)$ which originate from a structural distortion in the chain. This lattice distortion is probably related with the NMR results^{5,17} since the superlattice intensity also decreases gradually with increasing temperature. It should be pointed out that the x-ray experiments properly detected the coupling along the a axis but there is some disagreement along the c axis. As mentioned above, the structural distortion has correlations with two and four times periodicities along the c axis although magnetic dimers have correlations with five times periodicity. A discrepancy between magnetic and structural correlations was also reported in the spin-Peierls state in CuGeO_3 .³³ The magnetic excitations have a minimum energy at $(0,1,\frac{1}{2})$ but a superlattice reflection at $(\frac{1}{2},1,\frac{1}{2})$. An important point is that the x-ray results are for the ground state and neutron results are for the excited state.

We have shown that the dimer model shown in Fig. 7 explains the magnetic excitations reasonably well. The dimerized state is ascribed to the ordering of Cu^{2+} and ZR singlet which originates from an ordering of the localized holes. Hole ordering or charge ordering occurs in various 3d transition metal oxides. A quasi-two-dimensional hole ordering of the doped holes was reported in $\text{La}_2\text{NiO}_{4+\delta}$ ³⁴ and $\text{La}_{2-x-y}\text{Nd}_x\text{Sr}_y\text{CuO}_4$.³⁵ In the phase a static ordering of antiferromagnetic stripe is separated by charge ordered domain walls. In the latter compound the ordered phase can be described as a stripe ordering of Cu^{2+} and ZR singlet. Manganese oxides, for example $\text{La}_{1-x}\text{Ca}_x\text{MnO}_3$, also show a charge ordering of Mn^{3+} and Mn^{4+} .³⁶ In this system spin, charge, and orbital³⁷ degrees of freedom are closely

related, which results in interesting phenomena such as colossal magnetoresistance.³⁸ NaV_2O_5 , which consists of two-leg ladders of vanadium ions, has been studied extensively since it shows a singlet ground state below 34 K.³⁹ The phase transition was first considered to be a conventional spin-Peierls transition.⁴⁰ But the detailed inelastic neutron scattering experiment using single crystal sample revealed that the magnetic excitations in the dimerized phase could not be understood by a simple one-dimensional dimerized model.⁴¹ NMR experiment also indicated a charge ordering of V^{4+} and V^{5+} at the transition.⁴² Stimulated by these experimental findings, new approaches to understand the origin of the phase transition have been made theoretically.^{43,44} It is claimed that the transition is indeed closely related with a charge ordering of V^{4+} and V^{5+} ions. These various properties suggest that an intimate connection between hole/charge ordering and magnetic ordering is a common feature in the strongly correlated 3d transition metal oxides. Theoretical studies to explain the hole ordering and the dimerized state in $\text{Sr}_{14}\text{Cu}_{24}\text{O}_{41}$ are highly desirable.

B. Substitution effect in $\text{Sr}_{14-x}\text{Ca}_x\text{Cu}_{24}\text{O}_{41}$ ($x=3$)

We have also studied the substitution effect on the dimerized state. The dimerized state in the chain is most stable in pure $\text{Sr}_{14}\text{Cu}_{24}\text{O}_{41}$. When Y is substituted for Sr, the number of the holes is decreased and the number of the Cu^{2+} spins is increased. It was reported that Y substitution makes the magnetic excitation peaks broader.²⁹ As mentioned in Sec. I, the Ca substitution for Sr also reduces the number of the holes in the chain gradually.⁹⁻¹¹ Therefore, the Ca substitution is expected to affect the dimerized state in the chain.

Figure 10 shows typical inelastic neutron spectra at $(3,0,L)$ measured at 8 K in $\text{Sr}_{11}\text{Ca}_3\text{Cu}_{24}\text{O}_{41}$. The magnetic excitation peaks become broader with Ca substitution, which is similar to the case of Y substitution.²⁹ It is noted that two excitation branches are hardly resolved. However, the excitation energies are similar to those in $\text{Sr}_{14}\text{Cu}_{24}\text{O}_{41}$. The solid lines at $(3,0,-0.15)$, $(3,0,-0.30)$, and $(3,0,-0.35)$ are fits to two Gaussians and that at $(3,0,-0.75)$ is a fit to a single Gaussian by assuming that the dispersion relation is the same as that in $\text{Sr}_{14}\text{Cu}_{24}\text{O}_{41}$. The spectra are reasonably described with the simple model. As mentioned in Sec. III-A, the averaged excitation energy, the band width of each excitation mode, and the energy difference between the acoustic and optic modes are related with J , J_c , and J_a , respectively. This indicates that the coupling constants J , J_c , and J_a are almost unchanged with Ca substitution although the dimerized state becomes unstable. This behavior would be explained as the following. The hole ordering sensitively depends on the hole number. Accordingly, the long-range dimer formation becomes disturbed with Ca or Y substitution.

In $\text{Sr}_{14-x}\text{Y}_x\text{Cu}_{24}\text{O}_{41}$ system, magnetic excitations are remarkably affected with Y substitution.^{15,29} In the $x=0.25$ sample the excitation peaks become broader although the dispersion relation is almost unchanged. This result suggests that J , J_c , and J_a are almost unchanged although the hole ordering is disturbed with a small amount of Y. In the $x=1$ sample the excitation peaks become much broader, suggesting that the hole ordering becomes more unstable. An interesting behavior is that the averaged energy of the two excitations becomes reduced to ~ 9 meV, indicating that J is decreased in $\text{Sr}_{13}\text{Y}_1\text{Cu}_{24}\text{O}_{41}$. The changes of the bandwidth of each excited state, the difference in energy between two excited state, and the periodicity of the dispersion relation are difficult to be determined because the peaks are too broad to be resolved as two excitations. A puzzling feature is that J is decreased in $\text{Sr}_{13}\text{Y}_1\text{Cu}_{24}\text{O}_{41}$ although the lattice constant c , which affects the exchange constant, is almost independent of Y concentration.⁴⁵

When the holes are removed further, the hole ordering cannot be observed anymore and a long-range magnetic ordering appears.^{31,32,46} The CuO_2 chains in the hole removed $\text{Sr}_{14}\text{Cu}_{24}\text{O}_{41}$ can be considered as ferromagnetic spin chains which are weakly coupled with antiferromagnetic interchain coupling along the a and b axes.

In conclusion, neutron scattering experiments have been performed on $\text{Sr}_{14}\text{Cu}_{24}\text{O}_{41}$ in order to study the dimerized state in the CuO_2 chains. The ω - Q dispersion relation as well as the integrated intensities can be reasonably described by RPA calculation with $J=11$ meV, $J_c=0.75$ meV, and $J_a=0.75$ meV. The dimer configuration indicates a quasi-two-dimensional hole ordering, which results in an ordering of magnetic Cu^{2+} with $S = \frac{1}{2}$ and nonmagnetic ZR singlet. The hole ordering and the dimerized state are most stable in $\text{Sr}_{14}\text{Cu}_{24}\text{O}_{41}$. The Ca substitution for Sr sites makes the excitation peak broader probably because the hole ordering becomes unstable and the long-range dimer formation becomes disturbed.

ACKNOWLEDGMENTS

We would like to thank D. E. Cox, R. S. Eccleston, H. Eisaki, K. Katsumata, S. M. Shapiro, M. Takigawa, and A. Zheludev for stimulating discussions. This study was supported in part by the U.S.-Japan Cooperative Program on Neutron Scattering operated by the United States Department of Energy and the Japanese Ministry of Education,

- ¹ E. M. McCarron, III, M. A. Subramanian, J. C. Calabrese, and R. L. Harlow, *Mat. Res. Bull.* **23**, 1355 (1988).
- ² T. Siegrist, L. F. Schneemeyer, S. A. Sunshine, J. V. Waszczak, and R. S. Roth, *Mat. Res. Bull.* **23**, 1429 (1988).
- ³ R. S. Eccleston, M. Azuma, and M. Takano, *Phys. Rev. B* **53**, R14721 (1996).
- ⁴ K. Kumagai, S. Tsuji, M. Kato, and Y. Koike, *Phys. Rev. Lett.* **78**, 1992 (1997).
- ⁵ M. Takigawa, N. Motoyama, H. Eisaki, and S. Uchida, *Phys. Rev. B* **57**, 1124 (1998).
- ⁶ K. Magishi, S. Matsumoto, Y. Kitaoka, K. Ishida, K. Asayama, M. Uehara, T. Nagata, and J. Akimitsu, *Phys. Rev. B* **57**, 11533 (1998).
- ⁷ T. Imai, K. R. Thurber, K. M. Shen, A. W. Hunt, and F. C. Chou, *Phys. Rev. Lett.* **81**, 220 (1998).
- ⁸ E. Dagotto and T. M. Rice, *Science* **271**, 618 (1996).
- ⁹ M. Kato, K. Shiotani, and Y. Koike, *Physica C* **258**, 284 (1996).
- ¹⁰ Y. Mizuno, T. Tohyama, and S. Maekawa, *J. Phys. Soc. Jpn.* **66**, 937 (1997).
- ¹¹ T. Osafune, N. Motoyama, H. Eisaki, and S. Uchida, *Phys. Rev. Lett.* **78**, 1980 (1997).
- ¹² N. Motoyama, T. Osafune, T. Kakeshita, H. Eisaki, and S. Uchida, *Phys. Rev. B* **55**, 3386 (1997).
- ¹³ M. Uehara, T. Nagata, J. Akimitsu, H. Takahashi, N. Mori, and K. Kinoshita, *J. Phys. Soc. Jpn.* **65**, 2764 (1996).
- ¹⁴ F. C. Zhang and T. M. Rice, *Phys. Rev. B* **37**, 3759 (1988).
- ¹⁵ M. Matsuda, K. Katsumata, H. Eisaki, N. Motoyama, S. Uchida, S. M. Shapiro, and G. Shirane, *Phys. Rev. B* **54**, 12199 (1996).
- ¹⁶ R. S. Eccleston, M. Uehara, J. Akimitsu, H. Eisaki, N. Motoyama, and S. Uchida, *cond-mat/9711053*.
- ¹⁷ Y. Kitaoka *et al.* (private communication).
- ¹⁸ D. E. Cox, T. Iglesias, K. Hirota, G. Shirane, M. Matsuda, N. Motoyama, H. Eisaki, and S. Uchida, *Phys. Rev. B* **57**, 10750 (1998).
- ¹⁹ Z. Hiroi, S. Amelinckx, G. Van Tendeloo, and N. Kobayashi, *Phys. Rev. B* **54**, 15849 (1996).
- ²⁰ L. P. Regnault, H. Moudden, J. P. Boucher, J. E. Lorenzo, A. Hiess, and A. Revcolevschi, *The Annual Report of the Institute Laue-Langevin*, p.42, 1997.
- ²¹ T. Barnes, J. Riera, and D. A. Tennant, *cond-mat/9801224*.
- ²² Y. Sasago, M. Hase, K. Uchinokura, M. Tokunaga, and N. Miura, *Phys. Rev. B* **52**, 3533 (1995).
- ²³ A. Zheludev, G. Shirane, Y. Sasago, M. Hase, and K. Uchinokura, *Phys. Rev. B* **53**, 11642 (1996).
- ²⁴ D. A. Tennant, S. E. Nagler, A. W. Garrett, T. Barnes, and C. C. Torardi, *Phys. Rev. Lett.* **78**, 4998 (1997).
- ²⁵ A. W. Garrett, S. E. Nagler, D. A. Tennant, B. C. Sales, and T. Barnes, *Phys. Rev. Lett.* **79**, 745 (1997).
- ²⁶ The dispersion along the b axis is almost flat and the intensities along the b axis also monotonically decrease with increasing Q due to the magnetic form factor as reported in Ref. 15.
- ²⁷ B. Leuenberger, A. Stebler, H. U. Güdel, A. Furrer, R. Feile, and J. K. Kjems, *Phys. Rev. B* **30**, 6300 (1984).
- ²⁸ In Ref. 15 it was mentioned that the dispersion for the magnetic excitations at low- Q is almost flat along the a axis. The mistake was made because the measurements were performed mostly at H =integer.
- ²⁹ M. Matsuda, K. Katsumata, H. Eisaki, N. Motoyama, S. Uchida, T. Yokoo, S. M. Shapiro, G. Shirane, and J. L. Zarestky, *Phys. Rev. B* **56**, 14499 (1997).
- ³⁰ Y. Sasago, K. Uchinokura, A. Zheludev, and G. Shirane, *Phys. Rev. B* **55**, 8357 (1997).
- ³¹ M. Matsuda, K. Katsumata, T. Yokoo, S. M. Shapiro, and G. Shirane, *Phys. Rev. B* **54**, R15626 (1996).
- ³² M. Matsuda, K. M. Kojima, Y. J. Uemura, J. L. Zarestky, K. Nakajima, K. Kakurai, T. Yokoo, S. M. Shapiro, and G. Shirane, *Phys. Rev. B* **57**, 11467 (1998).
- ³³ K. Hirota, D. E. Cox, J. E. Lorenzo, G. Shirane, J. M. Tranquada, M. Hase, K. Uchinokura, H. Kojima, Y. Shibuya, and I. Tanaka, *Phys. Rev. Lett.* **73**, 736 (1994).
- ³⁴ J. M. Tranquada, D. J. Buttrey, V. Sachan, and J. E. Lorenzo, *Phys. Rev. Lett.* **73**, 1003 (1994).
- ³⁵ J. M. Tranquada, B. J. Sternlieb, J. D. Axe, Y. Nakamura, and S. Uchida, *Nature (London)* **375**, 561 (1995).
- ³⁶ E. O. Wollan and W. C. Koehler, *Phys. Rev.* **100**, 545 (1955).
- ³⁷ J. B. Goodenough, *Phys. Rev.* **100**, 564 (1955).
- ³⁸ P. Schiffer, A. P. Ramirez, W. Bao, and S.-W. Cheong, *Phys. Rev. Lett.* **75**, 3336 (1995).
- ³⁹ M. Isobe and Y. Ueda, *J. Phys. Soc. Jpn.* **65**, 1178 (1996).
- ⁴⁰ Y. Fujii, H. Nakao, T. Yoshihama, M. Nishi, K. Nakajima, K. Kakurai, M. Isobe, Y. Ueda, and H. Sawa, *J. Phys. Soc. Jpn.* **66**, 326 (1997).
- ⁴¹ T. Yoshihama, M. Nishi, K. Nakajima, K. Kakurai, Y. Fujii, M. Isobe, C. Kagami, and Y. Ueda, *J. Phys. Soc. Jpn.* **67**, 744

(1998).

⁴² T. Ohama, H. Yasuoka, M. Isobe, and Y. Ueda (preprint).

⁴³ H. Seo and H. Fukuyama, cond-mat/9805185.

⁴⁴ M. V. Mostovoy and D. I. Khomskii, cond-mat/9806215.

⁴⁵ M. Kato, T. Adachi, and Y. Koike, Physica C **265**, 107 (1996).

⁴⁶ S. A. Carter, B. Batlogg, R. J. Cava, J. J. Krajewski, W. F. Peck, Jr., and T. M. Rice, Phys. Rev. Lett. **77**, 1378 (1996).

FIG. 1. Structure of the CuO_2 chains (a) and the Cu_2O_3 ladders (b) in $\text{Sr}_{14}\text{Cu}_{24}\text{O}_{41}$. The lower part of the figure shows two dimer models as described in Section I: (c) Model I and (d) Model II. The squares denote Zhang-Rice singlet sites. Figure from ref. 18.

FIG. 2. Typical inelastic neutron spectra at $(H,0,L)$ at 15 K in $\text{Sr}_{14}\text{Cu}_{24}\text{O}_{41}$. The solid lines are the results of fits to a single Gaussian or two Gaussians.

FIG. 3. Observed and calculated energies (a) and intensities (b) at $(2,0,L)$ measured at 15 K in $\text{Sr}_{14}\text{Cu}_{24}\text{O}_{41}$. The solid and broken lines, which are fits to Eqs. (2) and (3), represent the acoustic and optic modes, respectively.

FIG. 4. Observed and calculated energies (a) and intensities (b) at $(3,0,L)$ measured at 15 K in $\text{Sr}_{14}\text{Cu}_{24}\text{O}_{41}$. The solid and broken lines, which are fits to Eqs. (2) and (3), represent the acoustic and optic modes, respectively.

FIG. 5. Observed and calculated energies (a) and intensities (b) at $(H,0,-0.2)$ measured at 15 K in $\text{Sr}_{14}\text{Cu}_{24}\text{O}_{41}$. The solid and broken lines, which are fits to Eqs. (2) and (3), represent the acoustic and optic modes, respectively.

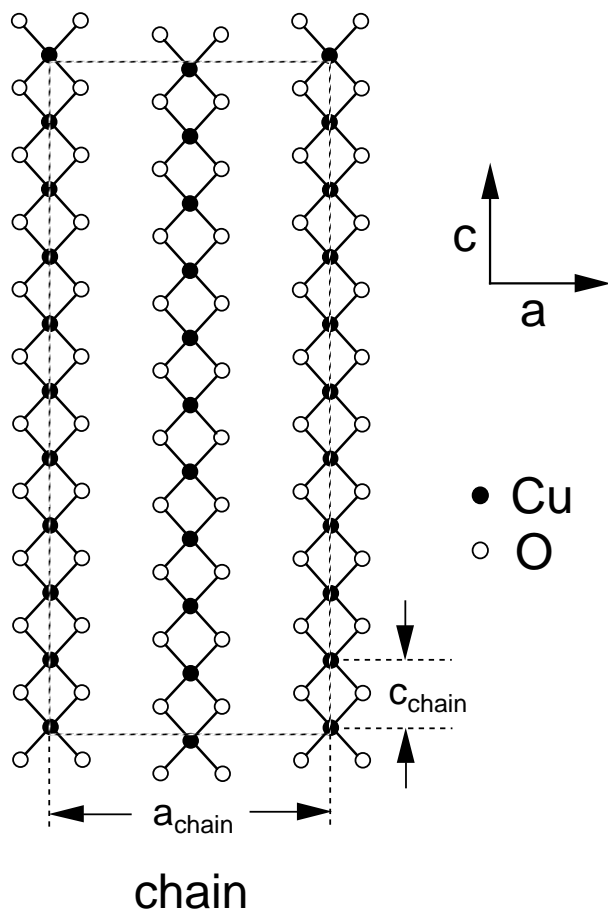
FIG. 6. Observed and calculated energies (a) and intensities (b) at $(H,0,-0.7)$ measured at 15 K in $\text{Sr}_{14}\text{Cu}_{24}\text{O}_{41}$. The solid and broken lines, which are fits to Eqs. (2) and (3), represent the acoustic and optic modes, respectively.

FIG. 7. A proposed model for the dimerized state and the ordering of Cu^{2+} and ZR singlet in the ac plane.

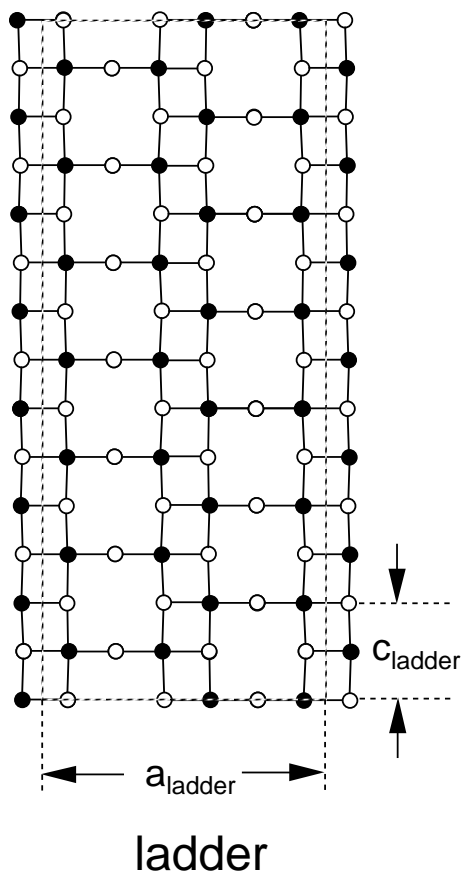
FIG. 8. Inelastic neutron spectra at $(2,0,-0.1)$ ($T=15$ and 75 K) and $(2,0,-0.6)$ ($T=15$ and 100 K) in $\text{Sr}_{14}\text{Cu}_{24}\text{O}_{41}$. The solid and broken lines are the results of fits to two Gaussians.

FIG. 9. Temperature dependence of the energy-integrated intensity and energy of the gap excitations at $(2,0,-0.1)$ and $(2,0,-0.6)$ in $\text{Sr}_{14}\text{Cu}_{24}\text{O}_{41}$. The solid lines are fits to Eqs. (2) and (3). The inset shows the calculated dispersion at 15 and 100 K.

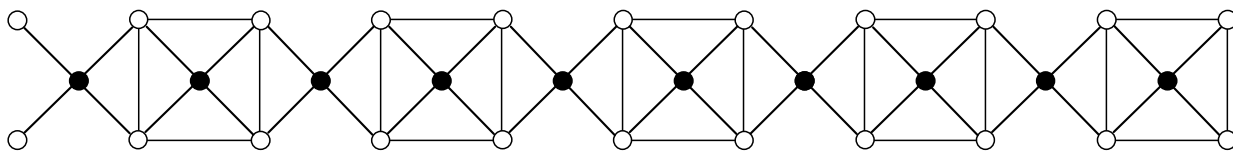
FIG. 10. Typical inelastic neutron spectra at $(3,0,L)$ at 8 K in $\text{Sr}_{11}\text{Ca}_3\text{Cu}_{24}\text{O}_{41}$. The solid lines are the results of fits to a single Gaussian or two Gaussians.



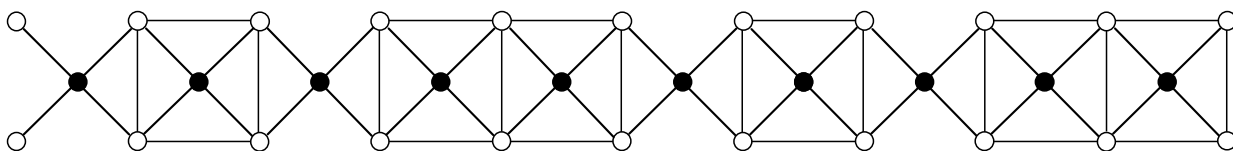
(a)



(b)

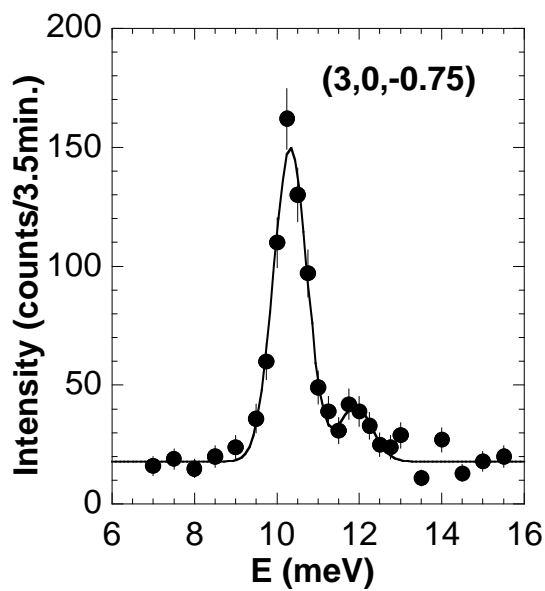
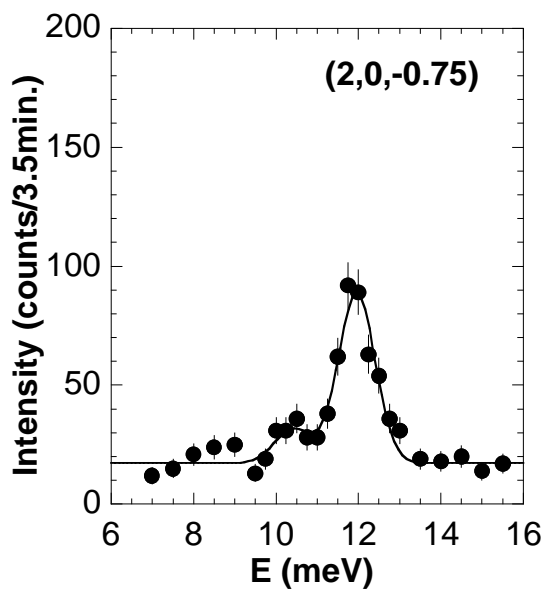
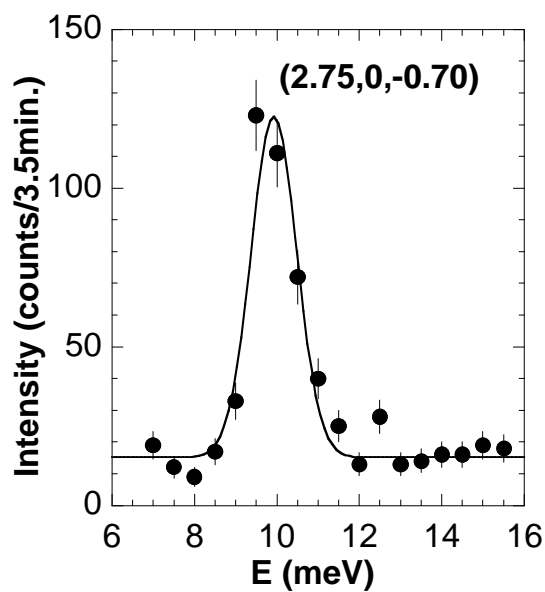
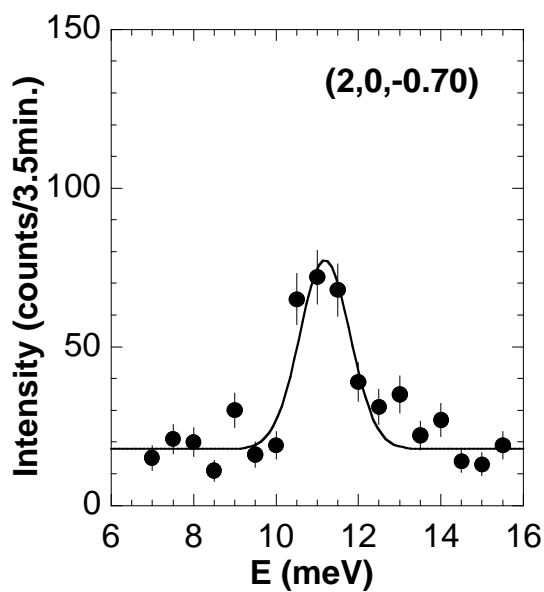
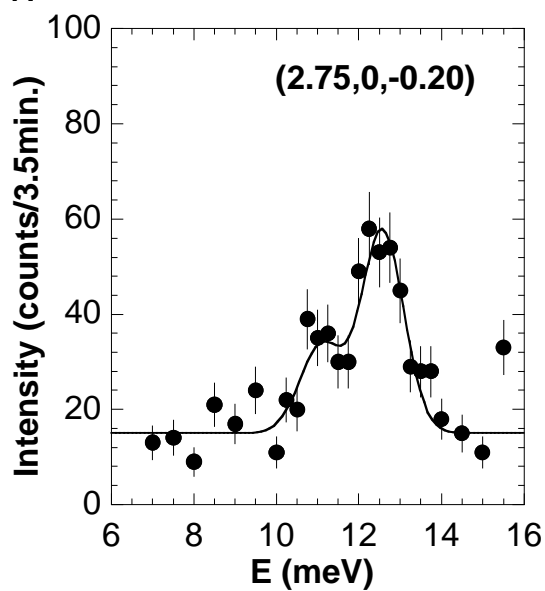
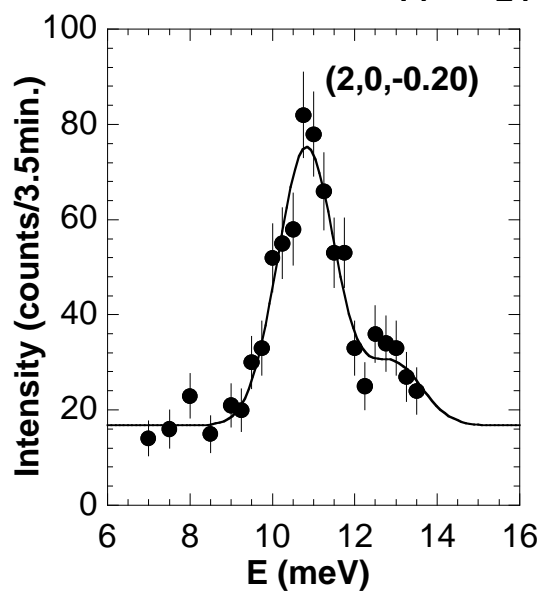


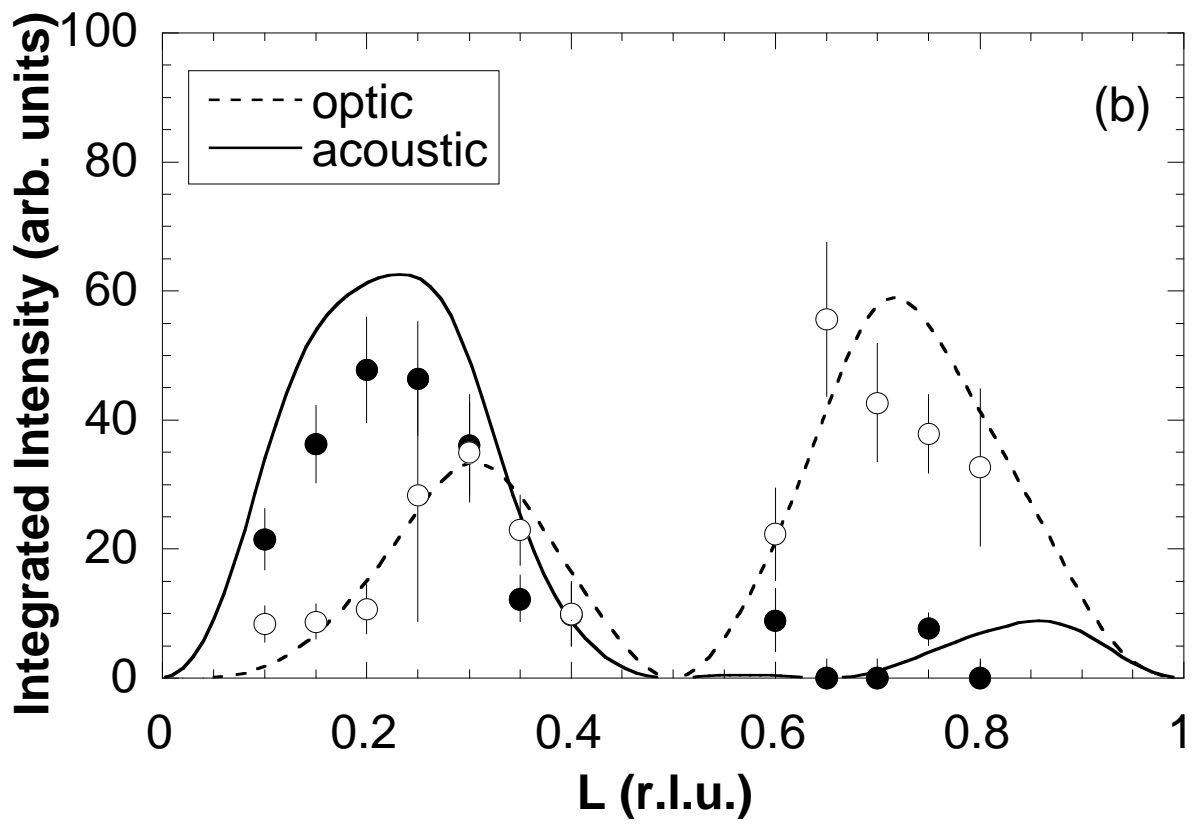
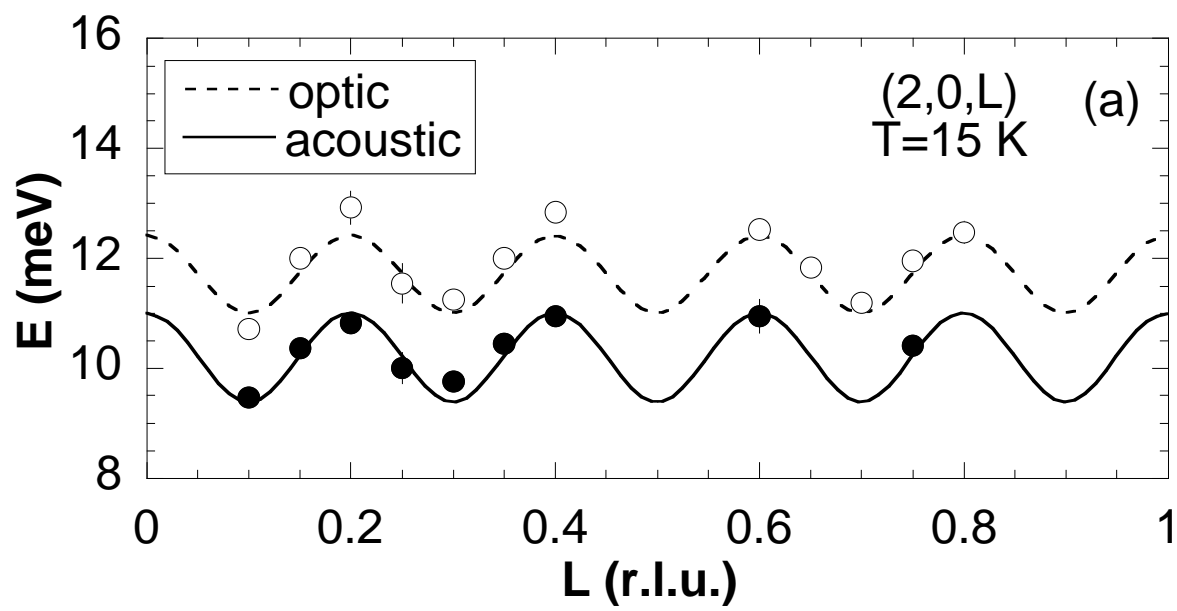
(c)

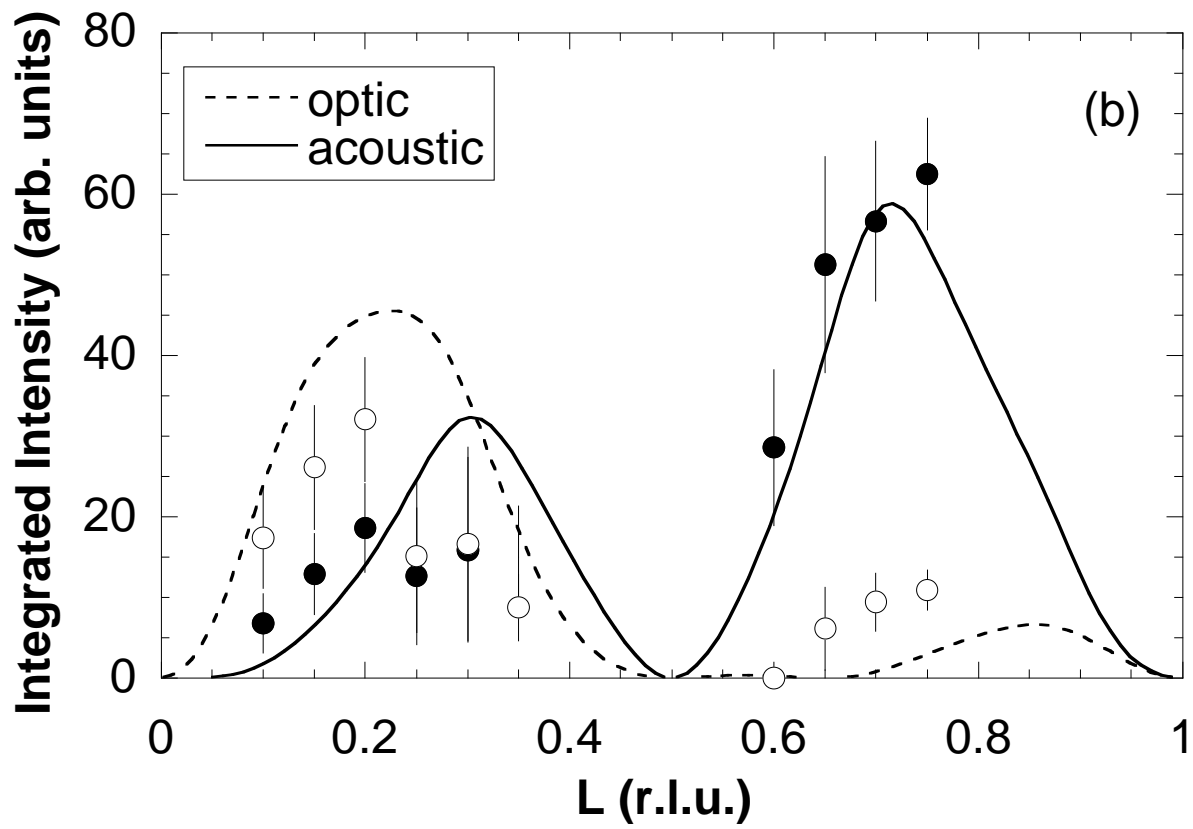
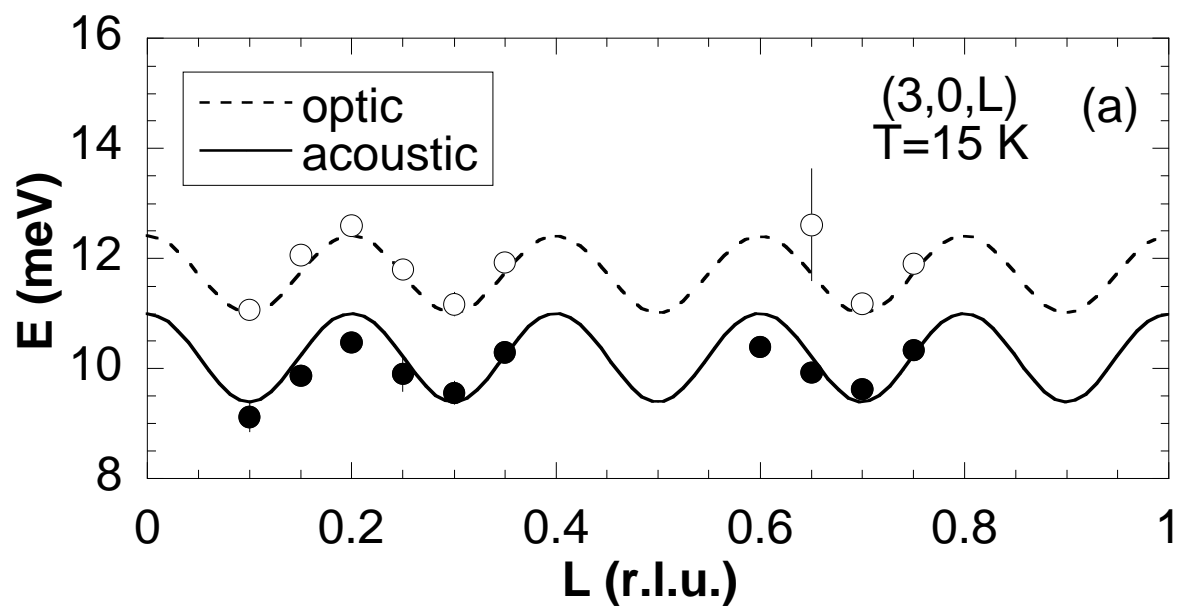


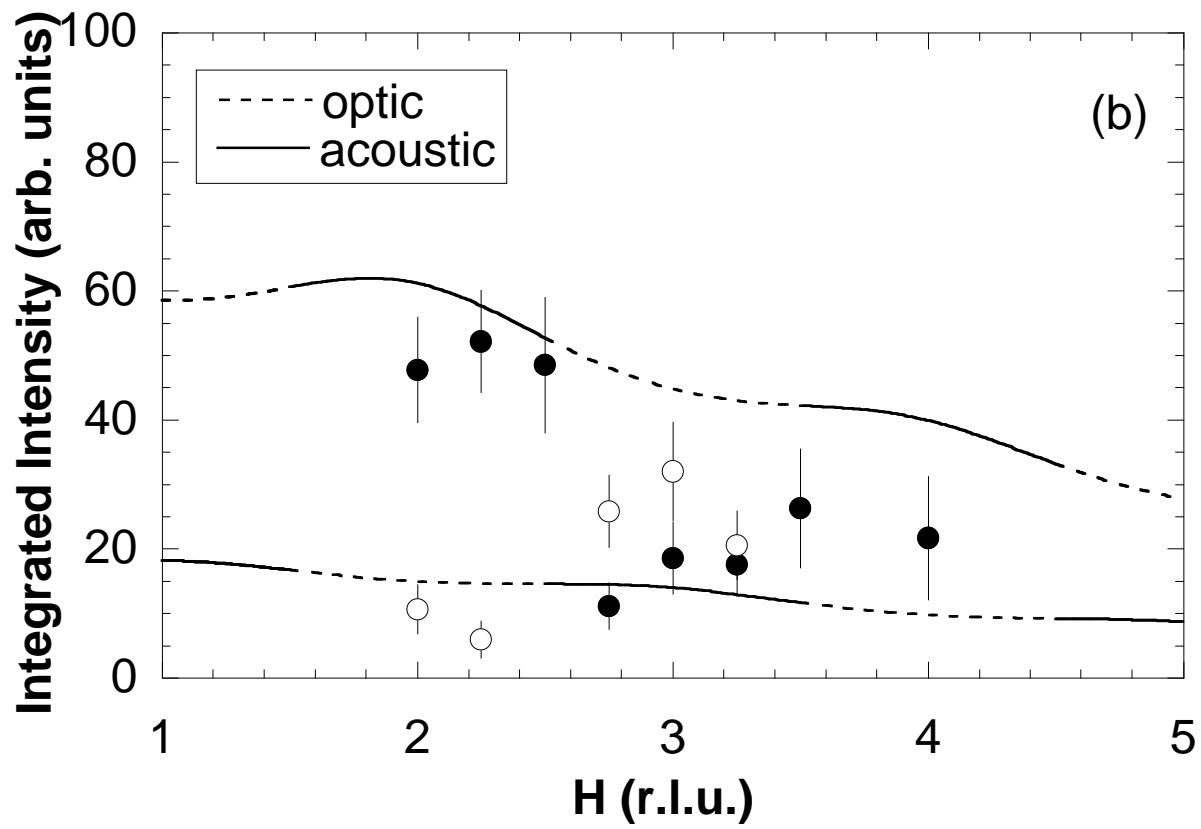
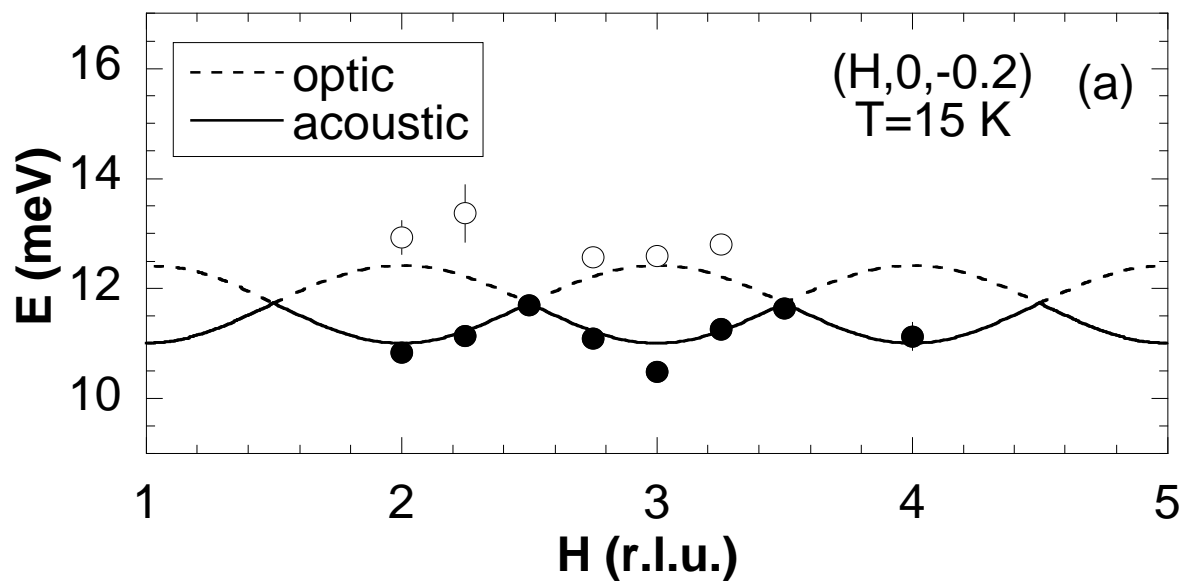
(d)

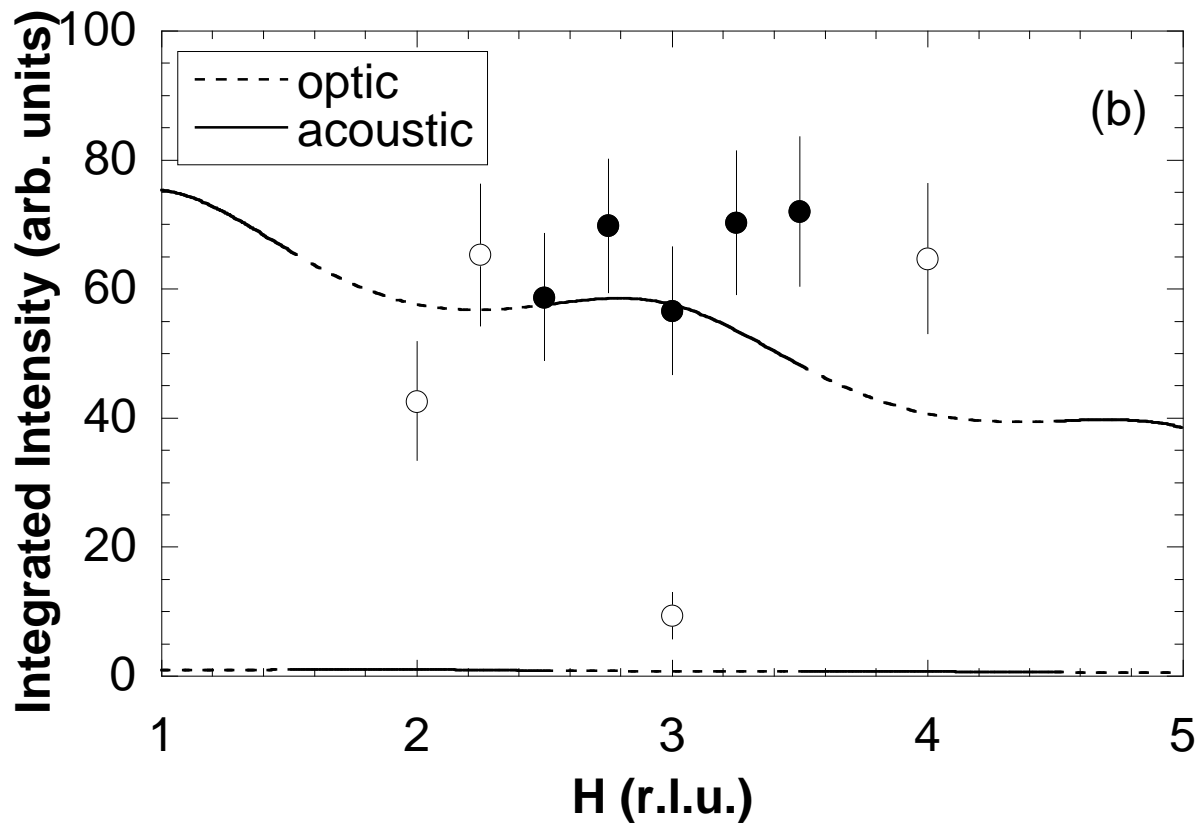
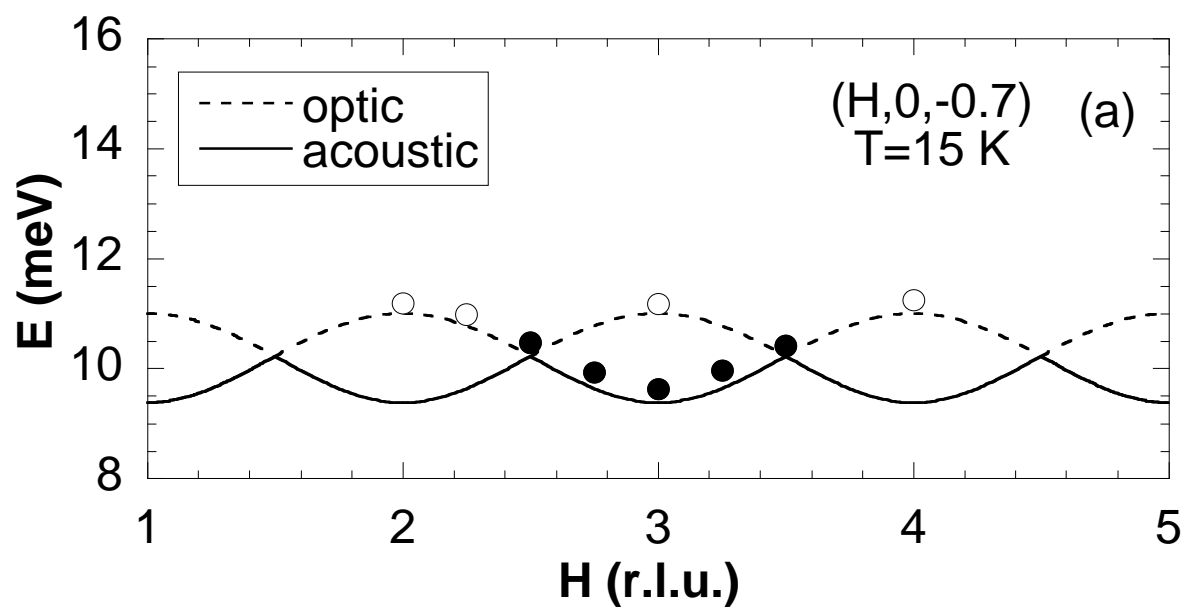
$\text{Sr}_{14}\text{Cu}_{24}\text{O}_{41}$ T=15 K

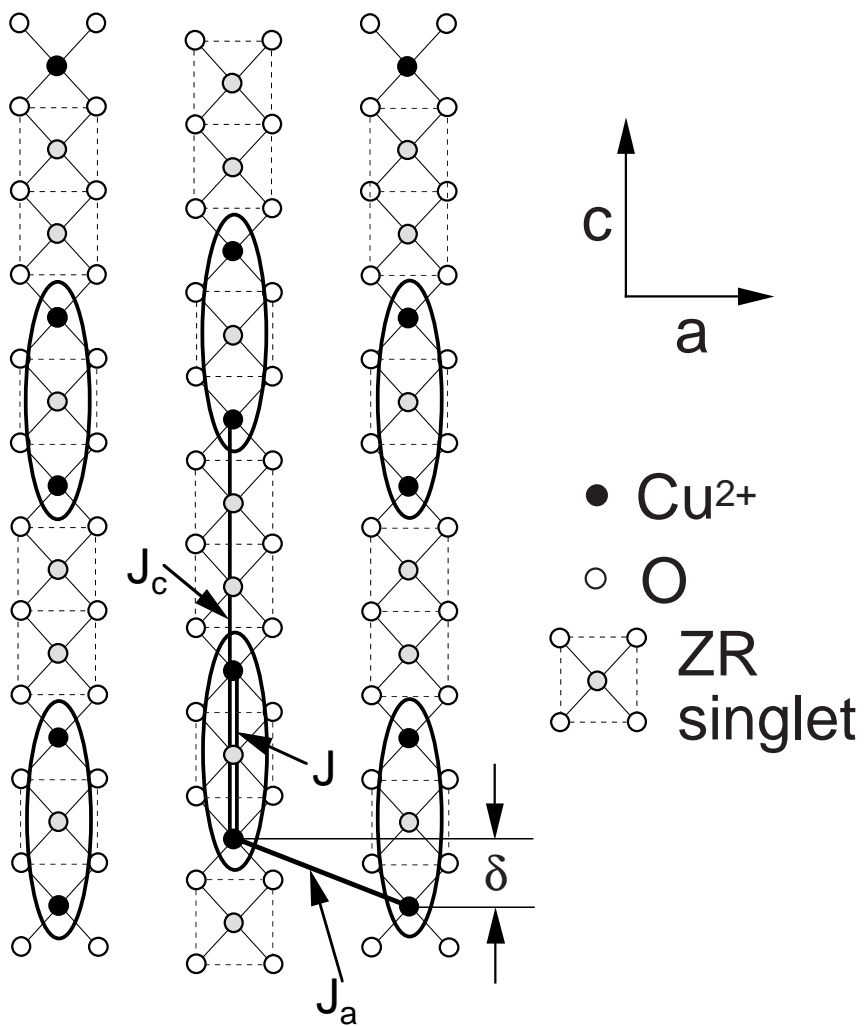


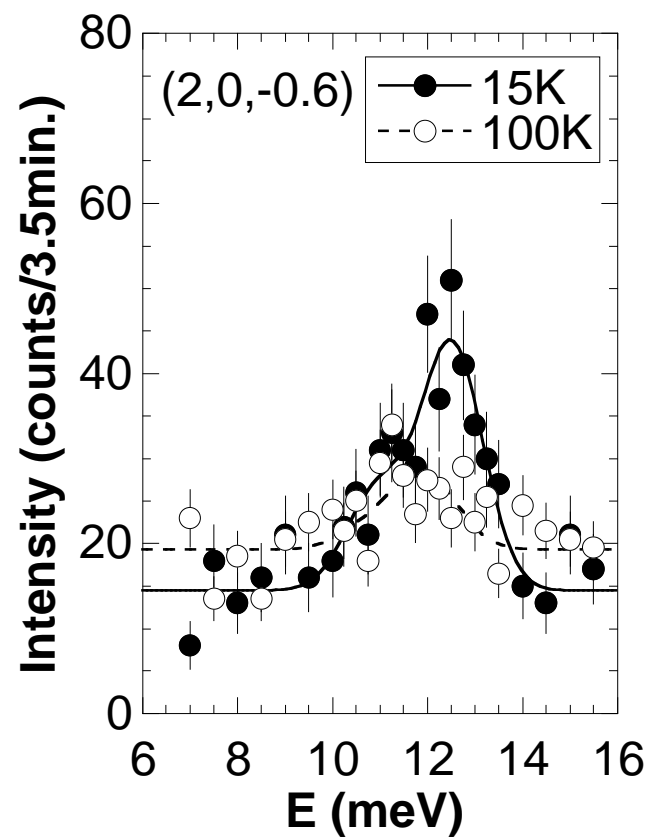
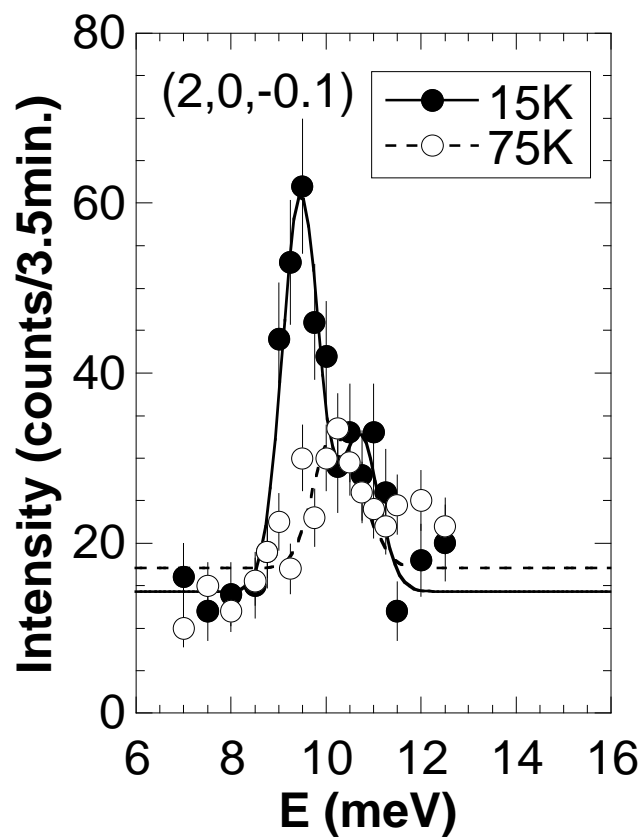


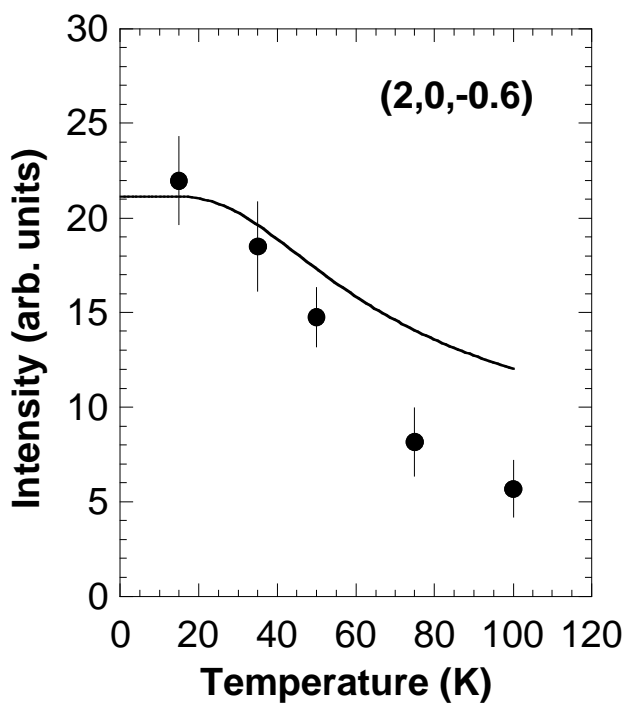
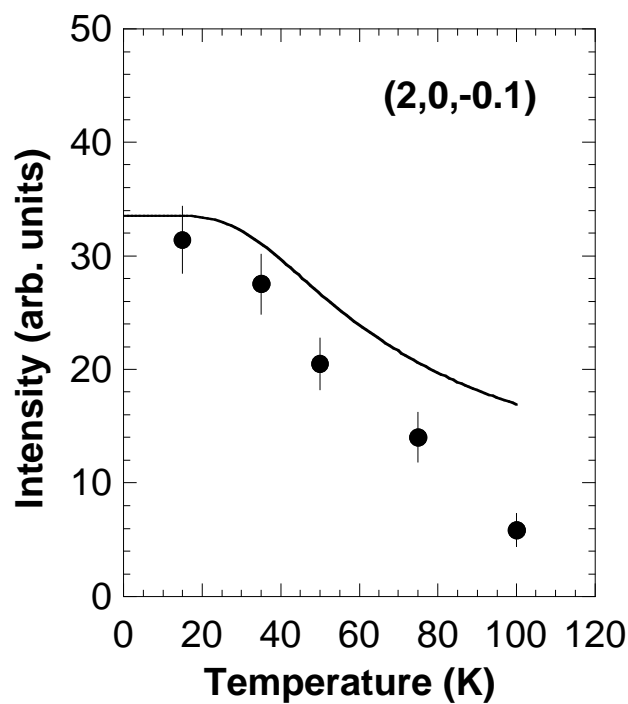
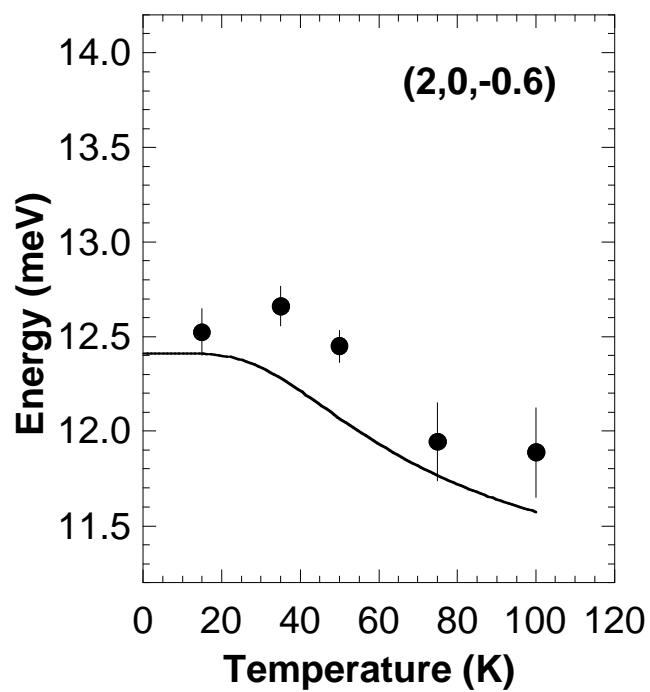
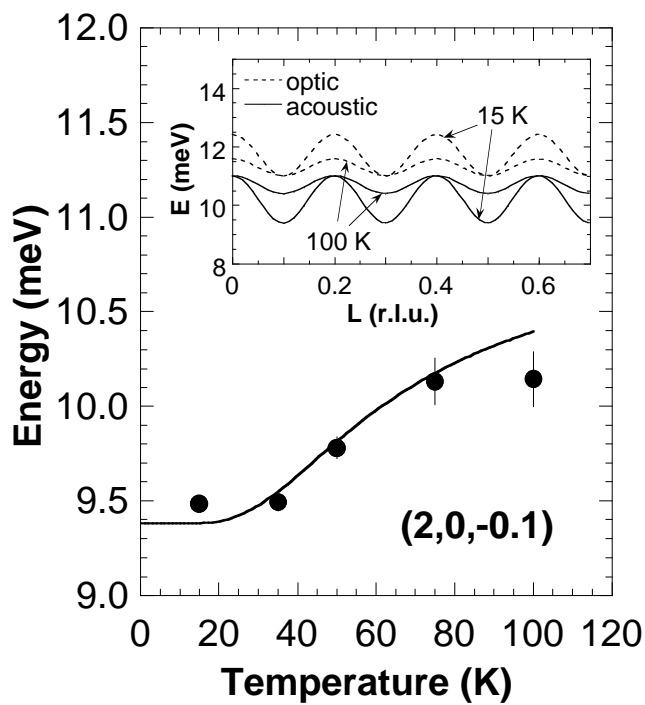












$\text{Sr}_{11}\text{Ca}_3\text{Cu}_{24}\text{O}_{41}$ T=8 K

